Experimental Study of Plane Spiral OAM Mode-Group Based MIMO Communications

Xiaowen Xiong, *Graduate Student Member, IEEE*, Shilie Zheng, *Member, IEEE*, Zelin Zhu, *Graduate Student Member, IEEE*, Yuqi Chen, *Graduate Student Member, IEEE*, Hongzhe Shi, Bingchen Pan, Cheng Ren, Xianbin Yu, *Senior Member, IEEE*, Xiaofeng Jin, Wei E. I. Sha, *Senior Member, IEEE*, and Xianmin Zhang, *Member, IEEE*

***Abstract*— Spatial division multiplexing using conventional orbital angular momentum (OAM) has become a well-known physical layer transmission method over the past decade. The mode-group (MG) superposed by specific single-mode plane spiral OAM (PSOAM) waves has been proved to be a flexible beamforming method to achieve the azimuthal pattern diversity, which inherits the spiral phase distribution of conventional OAM wave. Thus, it possesses both beam directionality and vorticity. In this article, it is the first time to show and verify a novel PSOAM MG based multiple-in–multiple-out (MG-MIMO) communication link experimentally in a line-of-sight (LoS) scenario. A compact multimode PSOAM antenna is demonstrated experimentally to generate multiple-independent controllable PSOAM waves, which can be used for constructing MGs. After several proof-of-principle tests, it has been verified that the beam directionality gain of MG can improve the receiving signal-to-noise ratio (SNR) level in an actual system. Meanwhile, the vorticity can provide another degree of freedom (DoF) to reduce the spatial correlation of MIMO system. Furthermore, a tentative long-distance transmission experiment operated at 10.2 GHz has been performed successfully at a distance of 50 m with a single-way spectrum efficiency of 3.7 bits/s/Hz/stream. The proposed MG-MIMO may have potential in the long-distance LoS backhaul scenario.**

***Index Terms*— Line of sight, mode group, multiple-in–multiple-out (MIMO) system, plane spiral orbital angular momentum (OAM), wireless communication.**

I. Introduction

THE capacity demand of wireless communication has been growing rapidly in the past decade, where 1 Tbits/s throughput has been expected to achieve in the next-generation wireless communication networks [1]. From the perspective of physical layer, various orthogonal resources have been investigated to improve the capacity performance, such as time, frequency, and space [2]. As a distinct space-division multiplexing technique, radio frequency (RF) orbital angular momentum (OAM) waves have been considered as one type of spatial orthogonal basis sets to achieve same-frequency mode-division multiplexing (MDM) [3], in which OAM waves present spiral phase front of $e^{-jl\varphi}$ (l is the OAM mode order) [4].

Since the famous *Venice Experiment* [5] was reported, a series of OAM-based MDM simulations or experiments in the line-of-sight (LoS) scenario has been published continually [6]–[11]. In [9], NTT Corporation has demonstrated an exhilarating work, in which they have successfully carried out an experiment of 100 Gbits/s OAM transmission at a distance of 100 m. Lei *et al.* [12] evaluated the throughput performance of OAM transmission in an indoor scenario, and the used OAM antenna can be found in [13]. Besides, OAM wave has been extended to other application fields, including radar imaging and detection [14], [15], eigenmode beamforming [16], [17], and rotational Doppler measurement [18].

Despite orthogonality between different OAM waves, it has been proved that the OAM MDM system could be summed up as a subset of multiple-in–multiple-out (MIMO) technique [19], but it still has a noteworthy superiority that signal processing complexity [8] can be reduced. In addition, the phase singularity [3] and the inherent divergence [20] of conventional OAM wave make it harder to receive the beam within a whole angular aperture. At present, there is a newly proposed MIMO architecture [21], [22] that OAM antennas are merely applied to the transmitting end, which utilizes the diversity of OAM waves rather than the orthogonality. According to [22], a special form of OAM wave called plane spiral OAM (PSOAM) wave has been adopted, each PSOAM wave propagates along the transverse direction ($\theta = 90°$), and the energy hole problem will no longer exist along the propagation axis. PSOAM wave's spiral phase distribution can provide a controllable degree of freedom (DoF) to decrease the spatial correlation between the subchannels [22]. However, due to the omnidirectivity in azimuthal direction of single-mode PSOAM wave, most of the energy is wasted, which could lead to the deterioration of signal-to-noise ratio (SNR) at the

Manuscript received March 1, 2021; revised June 8, 2021; accepted June 28, 2021. Date of publication July 26, 2021; date of current version January 11, 2022. This work was supported in part by the National Natural Science Foundation of China under Grant 61571391 and in part by the Zhejiang Lab under Grant 2020LC0AD01. *(Corresponding authors: Shilie Zheng; Xianmin Zhang.)*

Xiaowen Xiong, Shilie Zheng, Zelin Zhu, Yuqi Chen, Bingchen Pan, Cheng Ren, Xiaofeng Jin, and Wei E. I. Sha are with the College of Information Science and Electronic Engineering, Zhejiang University, Hangzhou 310027, China (e-mail: zhengsl@zju.edu.cn).

Hongzhe Shi is with Huawei Technologies Ltd., Shanghai 210206, China.

Xianbin Yu is with the Zhejiang Lab, Hangzhou 311121, China, and also with the College of Information Science and Electronic Engineering, Zhejiang University, Hangzhou 310027, China.

Xianmin Zhang is with the College of Information Science and Electronic Engineering, Zhejiang University, Hangzhou 310027, China, and also with the School of Information Science and Engineering, NingboTech University, Ningbo 315100, China (e-mail: zhangxm@zju.edu.cn).

Color versions of one or more figures in this article are available at https://doi.org/10.1109/TAP.2021.3098518.

Digital Object Identifier 10.1109/TAP.2021.3098518

receiving end. From the above, it is significant to find a feasible method to generate a directional beam, and meanwhile, such a directional beam should still retain a spiral phase distribution within its main lobe.

The beamforming can be realized by superposing eigenmodes of electromagnetic wave. Benefiting from the divergence consistency, PSOAM modes constitute a complete set of azimuthal eigenmodes. Superposing several specific PSOAM modes into a mode group (MG), a reconfigurable beamforming scheme can be implemented [16]. For conventional OAM waves, it is difficult to achieve due to the divergence inconsistency. PSOAM MG has its unique characteristics, including directionality, vorticity, and quasi-orthogonality [16]. It has been demonstrated that superposing consecutive PSOAM modes into an MG can realize a high-gain beam with a spiral phase distribution within its main lobe. As for such a high-gain beam, some researchers define it as quasi-OAM wave [23], [24]. However, since it contains multiple OAM mode components, thus, it would be more rigorous to call it MG [25]. PSOAM MG can be applied to the transmitting end to build the PSOAM MG based MIMO (MG-MIMO) system [26]. Fig. 1 shows the diagram of the proposed system, and the transmitting end could adopt the coaxial arraying way or the uniform linear arraying (ULA) way. So far, MG has evoked other unique applications of spatial field direct modulation [27], [28] and low interception communications [29].

In this article, the PSOAM MG based MIMO system has been experimentally verified for the first time, and it is the proof-of-concept experiments under laboratory conditions. A compact multimode PSOAM antenna has been designed to generate multiple PSOAM MGs simultaneously [17], which can be used for building the array at the transmitting end. The bit-error-rate (BER) performance of the proposed system is measured and analyzed in a veritable LoS scenario. The experimental results prove that MGs can increase the SNR and provide another DoF to decrease the spatial correlation, whereas, for conventional MIMO, the differences among subchannels are merely caused by the phase difference that is brought about by different propagation paths. Moreover, we have also demonstrated a trial long-distance wireless 16-quadrature amplitude modulation (QAM) transmission operated at 10.2 GHz, where the distance is 50 m (beyond the Rayleigh distance).

II. PSOAM MG Based MIMO Communication

A. Channel Model

In the proposed MG-MIMO [26], the PSOAM MG antennas are merely applied to the transmitting end, and the receiving end still uses the common antenna like the standard horn antenna to form a ULA. The proposed architecture takes advantage of the phase diversity of the MG rather than the orthogonality just like most of the OAM MDM systems do. As shown in Fig. 1, the channel model is illustrated as a 2×2 LoS-MIMO system to make it clear. For more general condition, when it comes to N MGs multiplexing, the number of horns should be equal to the number of multiplexing MGs. Based on the narrowband MIMO theory [19], [30], the general

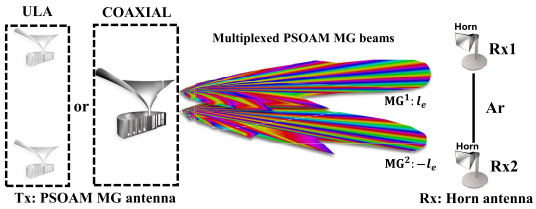

Fig. 1. Sketch map of 2×2 PSOAM MG based LoS-MIMO communication link. MG's main lobe possesses diversified and controllable phase information.

channel model of an $N \times N$ MG-MIMO system can be expressed as follows:

$$\begin{bmatrix} y_1 \\ y_2 \\ \vdots \\ y_N \end{bmatrix} = \begin{bmatrix} h_{11} & h_{12} & \cdots & h_{1N} \\ h_{21} & h_{22} & \cdots & h_{2N} \\ \vdots & \vdots & \ddots & \vdots \\ h_{N1} & h_{N2} & \cdots & h_{NN} \end{bmatrix} \begin{bmatrix} x_1 \\ x_2 \\ \vdots \\ x_N \end{bmatrix} + \begin{bmatrix} n_1 \\ n_2 \\ \vdots \\ n_N \end{bmatrix} \tag{1}$$

where $\mathbf{y} = [y_1, y_2, \ldots, y_N]^T \in \mathbb{C}^{N\times 1}$ is the complex receiving signal, $(\cdot)^T$ is the matrix transpose operation, $\mathbf{x} = [x_1, x_2, \ldots, x_N]^T \in \mathbb{C}^{N\times 1}$ is the complex transmitting signal, $\mathbf{n} = [n_1, n_2, \ldots, n_N]^T \in \mathbb{C}^{N\times 1}$ is the complex additive white Gaussian noise vector [31] at the receiving end, and $\mathbf{H} = [h_{mn}] \in \mathbb{C}^{N\times N}$ is the complex transfer matrix that consists of several transfer functions. Here, $\mathbf{H}$ can be either $\mathbf{H}^{\text{MIMO}}$ or $\mathbf{H}^{\text{MG}}$. To simplify the expression, we can write (1) as $\mathbf{y} = \mathbf{H}\mathbf{x} + \mathbf{n}$ [19].

The abovementioned transfer matrix is made up of several transfer functions, and given a propagation distance between a pair of transmitting and receiving antennas d_{mn}, $\mathbf{H}^{\text{MIMO}}$ can be expressed as

$$\mathbf{H}^{\text{MIMO}} = \beta_a \begin{bmatrix} \frac{\lambda e^{-jkd_{11}}}{4\pi d_{11}} & \cdots & \frac{\lambda e^{-jkd_{1N}}}{4\pi d_{1N}} \\ \vdots & \ddots & \vdots \\ \frac{\lambda e^{-jkd_{N1}}}{4\pi d_{N1}} & \cdots & \frac{\lambda e^{-jkd_{NN}}}{4\pi d_{NN}} \end{bmatrix} \tag{2}$$

where β_a contains all the antenna performance parameters, λ is the wavelength, $k = 2\pi/\lambda$ represents the free-space wavenumber, and $\lambda/(4\pi d)$ refers to the path loss. All transfer functions in $\mathbf{H}^{\text{MIMO}}$ mainly rely on the relative positions of transmitting and receiving array elements, which means that the differences between subchannels are merely caused by different propagation paths.

As for the MG-MIMO system, given a propagation distance d_{mn} from the nth MG antenna to the mth horn, its transfer matrix $\mathbf{H}^{\text{MG}}$ can be given as follows [26]:

$$\mathbf{H}^{\text{MG}} = \beta_a \begin{bmatrix} \frac{\lambda e^{-jkd_{11}}}{4\pi d_{11}} B P_{\text{MG}^1} & \cdots & \frac{\lambda e^{-jkd_{1N}}}{4\pi d_{1N}} B P_{\text{MG}^N} \\ \vdots & \ddots & \vdots \\ \frac{\lambda e^{-jkd_{N1}}}{4\pi d_{N1}} B P_{\text{MG}^1} & \cdots & \frac{\lambda e^{-jkd_{NN}}}{4\pi d_{NN}} B P_{\text{MG}^N} \end{bmatrix}. \tag{3}$$

In (3), $B P_{\text{MG}^n}$ is the term of the nth MG's beam pattern. This term represents that the MG antenna is used for the transmitting end instead of the common antenna. MG^n $\{l_f^n, l_f^n + \Delta l, \ldots, l_f^n + (Q-1)\Delta l\}$ is used to indicate an MG superposed by Q PSOAM modes $l = l_f^n$,

$l = l_f^n + \Delta l, \ldots, l = l_f^n + (Q-1)\Delta l$. Its beam pattern in polar coordinate can be expressed as follows:

$$BP_{\mathrm{MG^n}}(\varphi) = \frac{1}{\sqrt{Q}} \sum_{q=0}^{Q-1} A_q e^{-j\left[\left(l_f^n + q\,\Delta l\right)\varphi + \varphi_0^q\right]} \overset{\varphi_0^q = 0^\circ, A_q = 1}{=} \frac{1}{\sqrt{Q}} \frac{\sin\left(\frac{Q\varphi}{2}\Delta l\right)}{\sin\left(\frac{\varphi}{2}\Delta l\right)} e^{-j\left(l_f^n + \Delta l \frac{Q-1}{2}\right)\varphi} \quad (4)$$

where A_q and φ_0^q are the magnitude and initial phase of the qth PSOAM mode, respectively, l_f^n denotes the first PSOAM mode among the MG^n, the subscript f presents the first, Δl refers to the mode interval, and φ is the azimuthal angle; the constant $1/\sqrt{Q}$ is aimed at normalizing the power for a fairer comparison with conventional MIMO. For the situation of equiamplitude and in-phase, the beam pattern expression in (4) can be extended to the product of the amplitude term and the phase term. The amplitude term characterizes the directionality of an MG, which is related to Q and Δl. To realize a high-gain pencil beam, the mode interval Δl should be equal to 1, i.e., PSOAM modes in an MG must be consecutive modes. The phase term describes the spiral phase distribution within MG's main lobe, which is not only about Q and Δl but also about l_f^n. It is worth noticing that PSOAM MG can achieve azimuthal radiation pattern diversity [16].

1) *Directionality:* The PSOAM modes and the azimuthal angle constitute a Fourier transformation pair [32], and an MG with a high-gain beam has more components in the OAM mode spectrum, i.e., the beamwidth of an MG decreases with increasing Q [16].
2) *Vorticity:* The phase distribution within MG's main lobe is still linear to the azimuthal angle. The phase slope within the main lobe represents the vorticity of an MG. Here, we may define l_e^n as the equivalent OAM order of MG^n, which can be calculated from the phase term in (4)

$$l_e^n = l_f^n + \Delta l \frac{Q-1}{2}. \quad (5)$$

When both the transmitting and receiving ends obtain the channel state information (CSI) [33], i.e., once getting the transfer matrix shown in (2) or (3), the information-theoretic channel capacity limit can be calculated utilizing singular value decomposition (SVD) algorithm [26]

$$C = \sum_{k=1}^{rank(\mathbf{H})} \log_2\left(1 + \frac{\nu_k^2 P_k}{\sigma_n^2}\right) (bits/s/Hz)$$
$$\text{s.t.} \quad P_{total} = \sum_{k=1}^{rank(\mathbf{H})} P_k \quad (6)$$

where $\nu_k \in \{\nu_1, \nu_2, \ldots, \nu_{rank(\mathbf{H})}\}$ refers to the singular value decomposed by $\mathbf{H}$, σ_n^2 is the noise variance, and $rank(\cdot)$ represents the rank of a matrix. P_{total} is the total transmitting power and P_k is the power transmitted in the subchannels, where an optimized power allocation scheme called water-filling principle [34] can be adopted when CSI has been obtained. Given a receiving SNR, P_{total} can be estimated using the transfer function. After that, the capacity gain (CG) of MG-MIMO relative to single-in–single-out (SISO) system [19] could be simulated numerically.

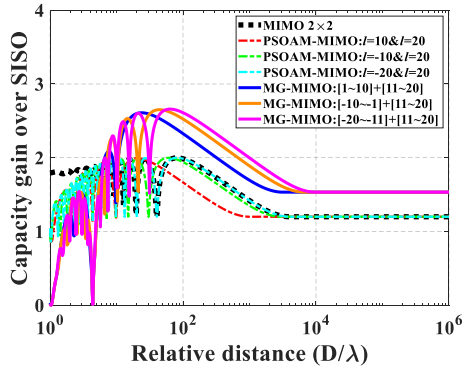

Fig. 2. CG over SISO system for conventional MIMO, PSOAM-MIMO, and MG-MIMO at the size 2×2. The receiving SNR is 30 dB. The Rayleigh distance [35] of $2A_r^2/\lambda$ is approximately 81.1λ.

TABLE I
SIMULATION PARAMETERS

Channel models	MIMO	PSOAM-MIMO	MG-MIMO
l_{max}	\	20	20
f_c[a]		10 GHz	
Receiving SNR		30 dB	
A_t[b]	$l_{max}\lambda/\pi$	Coaxial	Coaxial
A_r[c]	$l_{max}\lambda/\pi$	$l_{max}\lambda/\pi$	$l_{max}\lambda/\pi$

[a] f_c is the carrier frequency; [b] A_t is the transmitting aperture; and [c] A_t is the receiving aperture.

Fig. 2 shows the CG of conventional MIMO [19], PSOAM-based MIMO (PSOAM-MIMO) [22], and MG-MIMO in an LoS scenario, where the transmitting end of all the latter two systems takes the coaxial arraying way. Pivotal simulation parameters are given in Table I, where l_{max} is the maximum order PSOAM mode among multiplexing MGs and $l_{max}\lambda/\pi$ is the aperture of MG antenna, which makes sure to generate the lth-order PSOAM mode in theory [26]. The multiplexed MGs are MG^1 $\{1, 2, \ldots, 9, 10\}$, MG^2 $\{11, 12, \ldots, 19, 20\}$, MG^3 $\{-10, -9, \ldots, -2, -1\}$, and MG^4 $\{-20, -19, \ldots, -12, -11\}$. Each MG has the same certain directionality [16], and however, l_e^n of each MG is 5.5, 15.5, -5.5, and -15.5. In addition, the CG is simulated numerically at a receiving SNR of 30 dB no matter how long the communication distance D is.

The CG reaches its peak ever faster after a limited D, and then, it will deteriorate dramatically beyond the Rayleigh distance ($2A_r^2/\lambda$). Benefitting from the SNR improvement that MG's directionality brings, MG-MIMO has a better peak CG of about 2.6. Due to the consistent beam directionality of four MGs [16], the peak CG for the case of three pairs of multiplexed MGs remains the same. To obtain a specific CG such as 2, MG-MIMO can achieve a longer propagation distance, which is raised from 84λ of MIMO to 328λ (blue solid line, $\Delta l_e^{12} = 10$), 655λ (orange solid line, $\Delta l_e^{23} = 21$), and 993λ (magenta solid line, $\Delta l_e^{24} = 31$). Notably, for the same A_r and same directionality, if the difference value of equivalent OAM order Δl_e between multiplexed MGs is larger, the correlation of subchannels will be lower, which verifies

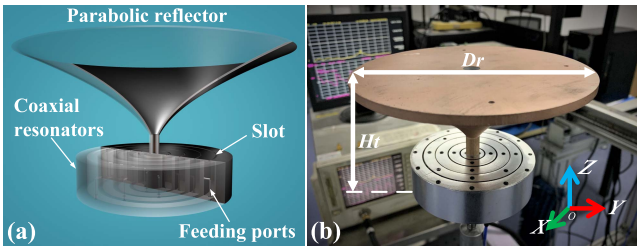

Fig. 3. (a) Cross view of the mentioned PSOAM MG antenna. (b) Picture of the fabricated antenna.

numerically that MGs provide a controllable DoF to decrease the spatial correlation.

As for the PSOAM-MIMO, without the SNR improvement, the peak CG of PSOAM-MIMO is the same as MIMO system about 2. As the difference value of OAM order Δl between multiplexed PSOAM waves increases, the propagation distance will also increase. However, because the subchannel difference caused by coaxially arraying PSOAM waves is weaker than that caused by the propagation path, its communication distance is even shorter than MIMO for a certain CG. If the transmitting end of PSOAM-MIMO adopts the ULA arraying way, it would show a better performance of communication distance [22].

B. Transmitting End: PSOAM MG Antenna

For the sake of constructing the proposed MG-MIMO communication link, a PSOAM MG antenna that can simultaneously radiate several required MGs needs to be manufactured. To achieve such a goal, a compact multimode PSOAM antenna has been demonstrated [17]. The proposed antenna is made up of four coaxial resonators and a parabolic reflector. The cross-sectional view and the real picture of the antenna are shown in Fig. 3. The total height H_t of MG antenna is 80 mm and the diameter of reflector D_r is 150 mm, so the physical aperture of such an antenna (the diagonal length of cross section) is approximately 170 mm (about 5.8λ).

In virtue of the 90° hybrid coupler [36], in the same resonator, the $\pm l$ order PSOAM waves can be excited concurrently [7]. Therefore, such an antenna could synchronously generate eight PSOAM waves with the OAM order $l = \pm 1, \pm 2, \pm 3$, and ± 4, and in the following experiments, all the PSOAM modes are used at 10.2 GHz. Only the four typical examples are presented, and their measured phase and normalized intensity distributions in the transverse plane are shown in Fig. 4. The results display the distinct feature of single-mode PSOAM wave. Obviously, the central singularity of PSOAM waves will exist inside the antenna itself, and the energy hole problem can be reasonably avoided. The phase changes $2\pi l$ along the circumference. The inhomogeneity of the intensity is caused by the errors of manufacture and the energy loss of resonant cavity [36], [37], and the latter factor results in the more serious inhomogeneity for the higher order PSOAM mode.

Besides, each PSOAM wave can be manipulated independently relying on an amplitude–phase controllable feeding network, which can realize the generation of MG. Fig. 5(a) shows the measured far-field directivity and phase distribution

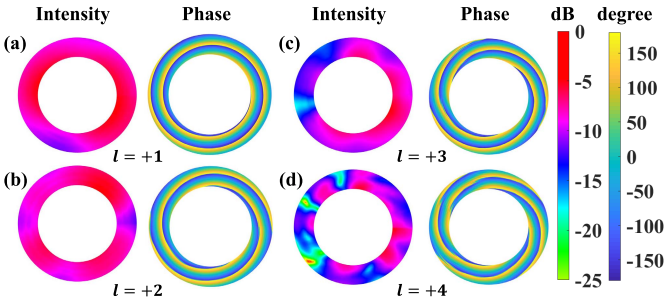

Fig. 4. Measured near-field results including the phase and the normalized intensity distributions in the transverse plane of PSOAM waves. (a) $l = 1$. (b) $l = 2$. (c) $l = 3$. (d) $l = 4$.

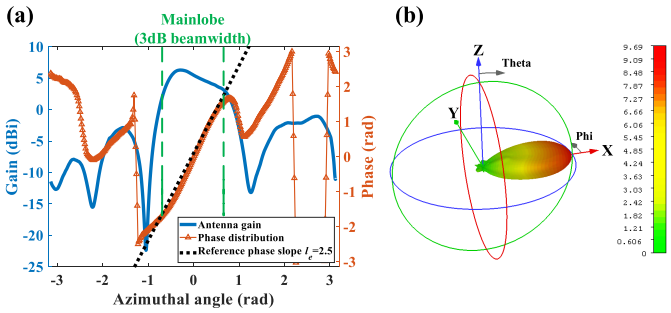

Fig. 5. (a) Measured far-field directivity (blue line) and phase distribution (dark orange line) for MG {1, 2, 3, 4} at XOY plane ($\theta = 90°$). (b) Simulated 3-D far-field pattern (linear scale) for MG {1, 2, 3, 4}.

of MG {1, 2, 3, 4} at $\theta = 90°$ plane. The main lobe magnitude and 3 dB beamwidth of azimuthal angle are 6.3 dBi and 71°, respectively. The measured phase within the main lobe presents a linear distribution with respect to azimuthal angle. Therefore, it proves that MG possesses the directionality and the vorticity at the same time. The linearity of phase slope is about good, and the estimation value of l_e is 2.5, which is in good agreement with the theoretical reference value (black). In addition, the simulated 3-D far-field pattern is shown in Fig. 5(b), and it can be seen more visually that a high-gain pencil beam can be generated in the transverse plane. Additional design parameters and electrical performance about this antenna can be found in [17].

C. Communication System Architecture

A schematic overview of an $N \times N$ PSOAM MG based MIMO system is shown in Fig. 6(a). For the transmitting module, in virtue of orthogonal frequency-division multiplexing (OFDM) [30] technique with 56 subcarriers, N-way independent modulated baseband signals with the 20 MHz bandwidth (BW) whose intermediate frequency (IF) is set as 800 MHz are generated by a software-defined radio (SDR; V3 Technology YunSDR Y410s) [38] platform. The modulation formats are quadrature phase shift keying (QPSK), 16-QAM, and 64-QAM [31]. N-way IF signals are fed to the IF ports of N mixers, and N-way 9.4 GHz continuous-wave (CW) signals [local oscillator (LO)] are fed to the LO ports of N mixers; so far, the baseband signals are upconverted to the carrier frequency f_c of 10.2 GHz and these RF signals are exported from the RF ports of N mixers. Then, after getting through the bandpass filters (BPFs) and power amplifiers

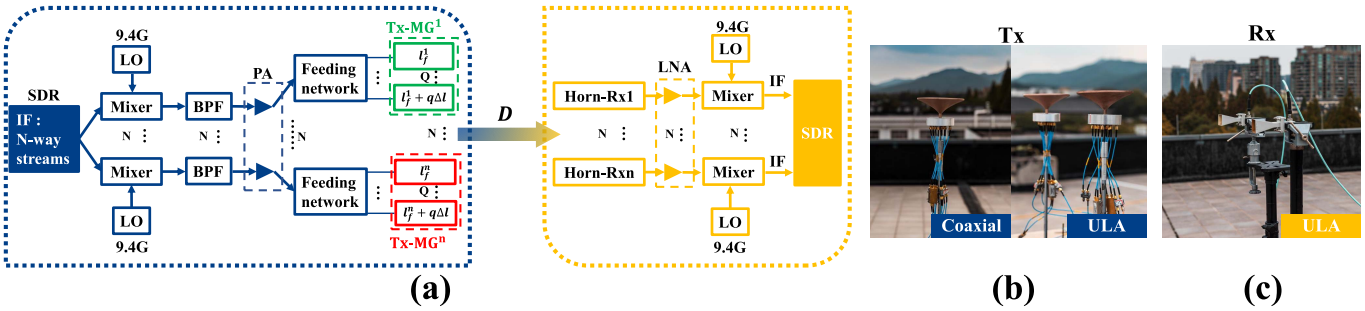

Fig. 6. (a) Schematic of an $N \times N$ MG-MIMO communication architecture in an LoS scenario with a communication distance D. The N PSOAM MGs carrying N data streams are used for the transmitting end, in which the carrier frequency f_c is 10.2 GHz. SDR: software-defined radio. IF: intermediate frequency signal. LO: local oscillator. BPF: bandpass filter. PA: power amplifier. Tx/Rx: transmitting antenna and receiving antenna. Horn: standard gain horn antenna. LNA: low-noise amplifier. Taking a 2×2 MG-MIMO communication link as an example, (b) transmitting end can adopt the coaxial arraying way or the ULA arraying way utilizing the proposed MG antennas and (c) receiving end adopts the ULA arraying way utilizing the horn antennas.

(PAs), N-way RF signals carrying data streams are fed to the amplitude–phase controllable feeding networks. Each feeding network consists of a power divider, electrically tuned phase shifters, electrically tuned attenuators, and a digital-to-analog converter (DAC) circuit (DAC81416, Texas Instruments) used for realizing the voltage control, which is used to manipulate the intensity and the initial phase of each PSOAM wave among an MG. More details about the mentioned feeding network can be found in [17]. Combining the feeding networks and the proposed MG antennas, N MGs carrying N-way independent data streams can be radiated and multiplexed in free space. Since the MG antenna can simultaneously generate eight different PSOAM modes, these modes could be divided into multiple MGs, and hence, it is possible for the transmitting end to adopt the coaxial arraying way in addition to the ULA arraying way. Fig. 6(b) shows the experimental setup. In a sense, the coaxial arraying way can be considered that N multiplexed MGs radiate from the origin in a polar coordinate.

After a free-space transmission in an LoS scenario, N-way RF signals carrying data streams reach the receiving horn antennas. On account of the path loss, in order to meet the certain SNR requirement, the receiving signals need to be amplified by the low-noise amplifiers (LNAs). Following by passing through the mixers, the RF signals are downconverted to the IF signals (800 MHz). Then, the IF signals are fed to the SDR platform to realize the process of signal demultiplexing, in which the second amplification and the second downconversion are operated to get the digital baseband signals. Finally, the transmitted modulated signals can be recovered, and the BER, received constellation diagrams, and error vector magnitude (EVM) performance could be analyzed. Importantly, the MIMO demultiplexing algorithm used in SDR platform is zero-forcing [39] algorithm. Besides, as shown in Fig. 6(c), the receiving end takes the ULA arraying way to form an antenna array utilizing standard gain horn antennas.

III. Proof-of-Principle Experiments

Limited by the number of channels available for our SDR platform, in the following several experiments, we set up a 2×2 MG-MIMO prototype to demonstrate and analyze the related communication performance.

Fig. 7. Experimental setup used to study the impact on communication link performance of MG's vorticity.

A. Impact on Link Performance of MG's Vorticity

It has been verified the validity numerically that, for the same A_r and same directionality of MGs, if Δl_e between multiplexed MGs is larger, the correlation of subchannels will be lower. To eliminate the subchannel difference caused by the different propagation paths, the transmitting end adopts the coaxial arraying way, and here, the subchannel difference is merely brought by the linear phase distribution of MGs. At the receiving end, two horn antennas are placed at the symmetry positions along the propagation axis. The aperture of the receiving ULA A_r is set to 0.6 m, and the communication distance D is 5 m, as shown in Fig. 7. In addition, the total number Q of PSOAM modes in each MG needs to stay the same [16], and therefore, the beam gain (directionality) of each MG can stay almost the same, which makes sure that the receiving SNR can remain consistent for each control group. Four pairs of MGs used for conducting the comparison experiments are $\mathrm{MG}^1\{-1, 1\}$ and $\mathrm{MG}^2\{-2, 2\}$ with Δl_e of 0 (a pair of plane waves [16]), $\mathrm{MG}^3\{1, 2\}$ and $\mathrm{MG}^4\{-2, -1\}$ with Δl_e of 3, $\mathrm{MG}^5\{2, 3\}$ and $\mathrm{MG}^6\{-3, -2\}$ with Δl_e of 5, and $\mathrm{MG}^7\{3, 4\}$ and $\mathrm{MG}^8\{-4, -3\}$ with Δl_e of 7.

To observe the characteristic in frequency domain of the received signals, Fig. 8(a) and (b) shows the typical received power spectral density (PSD) of the QPSK transmission at an SNR of 28 dB and the 16-QAM transmission at an SNR of 30 dB, respectively. Such a spectrum can be achieved by using the fast Fourier transformation (FFT) to do the calculation of the received baseband signal, where the signal is sampled by the 12-bit analog-to-digital converter (ADC)

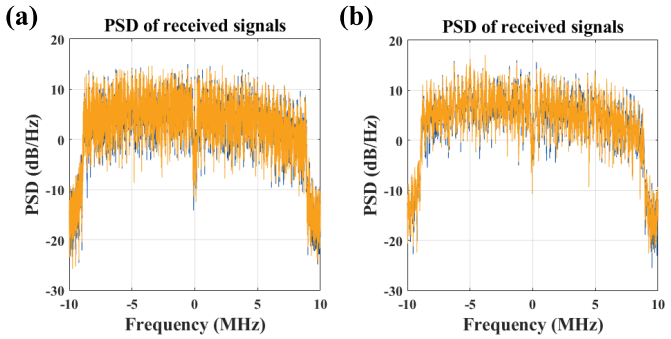

Fig. 8. Typical PSD of the received signals at the receiving SNR of (a) 28 dB in the QPSK transmission link and (b) 30 dB in the 16-QAM transmission link.

in our SDR platform. As we can see, the central subcarrier of a typical OFDM symbol with the BW of 20 MHz is set to the null in order to overcome the problem of direct-current (dc) shift [40], [41]. Here, an OFDM symbol contains 56 subcarriers, of which 52 subcarriers can be used for data transmission. The subcarrier interval is 312.5 kHz.

The measured raw BER curves of the QPSK transmission and the 16-QAM transmission are shown in Fig. 9(a) and (c), respectively. Fig. 9(b) shows the typical received constellations with the EVM performance of the QPSK transmission at a receiving SNR of 28 dB for each pair of multiplexed MGs. Similarly, Fig. 9(d) shows the corresponding results in the case of 16-QAM transmission at a receiving SNR of 30 dB. When the receiving aperture A_r, the total number Q, and the communication distance D are, respectively, fixed as 0.6 m, 2, and 5 m, for both two modulation formats, as Δl_e increases from 0, 3, 5, and 7, the corresponding BER value is reduced to a certain extent, i.e., the communication performance is getting better for the case of larger Δl_e. It is important and worthy of attention that, here, the difference of subchannels is entirely caused by the MG's linear phase distribution rather than the propagation path difference like MIMO technique does. Due to the coaxial arraying way at the transmitting end, for the receiving horns arranged symmetrically along the propagation axis, the wave path of two plane waves carrying data streams to the two receiving antennas is almost the same, which means that there is no spatial diversity [42] between the multiplexed signals. At this time, the system cannot support the multiplexing, severe aliasing occurs between the multiplexed signals, and its received constellations are shown in Fig. 9(b) and (d). As a consequence, for the case of $\Delta l_e = 0$, its BER values at each SNR for both modulation formats are all above the level of 20%, and it is an intolerable level in wireless communication system [30].

In the case of the QPSK transmission, as far as the test results are concerned, when Δl_e is 5 or 7, the MG-MIMO system can reach a raw BER level of 3.8×10^{-3}, which is a level allowing extremely low error rates in virtue of efficient forward error correction (FEC) codes [31]. Benefiting from the lower subchannel correlation, the multiplexing of MG^7 and MG^8 can reach the FEC limit at a lower SNR of about 26 dB, and the multiplexing of MG^5 and MG^6 needs a 28 dB SNR to reach the same limit. At the same receiving SNR of 28 dB, the EVM performance of two channels for $\Delta l_e = 3$, $\Delta l_e = 5$, and $\Delta l_e = 7$ are 36.2% and 30.0%, 29.3% and 23.2%, and 17.0% and 15.5%, respectively.

As for the 16-QAM transmission, similarly, when Δl_e is 5 or 7, the MG-MIMO system can reach the FEC limit. The multiplexing case of $\Delta l_e = 7$ reaches the FEC limit at a lower SNR of about 28 dB, and the multiplexing case of $\Delta l_e = 5$ requires a higher SNR of 30 dB to reach this limit. At a certain receiving SNR of 30 dB, the EVM performance of two channels for $\Delta l_e = 3$, $\Delta l_e = 5$, and $\Delta l_e = 7$ are 20.5% and 19.3%, 14.5% and 15.6%, and 15.2% and 15.0%, respectively.

B. Impact on Link Performance of MG's Directionality

The PSOAM-MIMO system [22] also utilizes the diversity of PSOAM waves rather than the orthogonality, where the diversity is given by PSOAM wave's azimuthal spiral phase distribution. Unfortunately, because of the omnidirectivity (as shown in Fig. 4) in azimuthal direction of single-mode PSOAM wave, most of the energy is wasted, which will result in the deterioration of the receiving SNR. The beam generated by the PSOAM MG technique can realize the azimuthal beamforming to achieve the convergence of energy. In order to compare MG-MIMO with PSOAM-MIMO, to refer to the experimental setup in [22], the transmitting and receiving ends will employ the ULA arraying way, A_t and A_r are all set as 0.35 m. In order to fully demonstrate the beam gain superiority of MG over single-mode PSOAM wave, as shown in Fig. 10, the communication distance D of this outdoor experiment is set to be longer, where D is 25 m. To strictly control the variable, the mode interval Δl between multiplexed single-mode PSOAM waves should be equal to Δl_e between multiplexed MGs. For the proposed MG-MIMO, the multiplexed MGs are MG$\{-4, -3, -2, -1\}$ and MG$\{1, 2, 3, 4\}$ with Δl_e of 5. As for the PSOAM-MIMO, the multiplexed single-mode PSOAM waves are $l = +2$ and $l = -3$. In addition, when the MG antenna is used for radiating single-mode PSOAM wave, the RF signals carrying data streams can be directly fed into the ports of corresponding PSOAM modes without going through the feeding network, and meanwhile, the remaining ports of the MG antenna are terminated with several matching loads. By contrast, for the proposed MG-MIMO, a higher insertion loss is going to be introduced actually.

Fig. 11(a) shows the measured raw BER curves of MG-MIMO and PSOAM-MIMO system for the QPSK transmission. In contrast to the PSOAM-MIMO, the MG-MIMO shows a better BER capability in a remote wireless communication scenario. At a receiving SNR of 22.4 dB, MG-MIMO can reach the FEC limit, and PSOAM-MIMO needs a receiving SNR of 25 dB to reach the same limit. For both the systems, when the power of transmitting IF signal, the LO power, and the gain of receiving LNA are, respectively, set as -24 dBm, 10 dBm, and 67 dB, the attainable SNR of MG-MIMO link is 30.7 dB, and this value of PSOAM-MIMO is only 25 dB, which profits from that the MG constructed by four PSOAM waves has an azimuthal beam gain of about 6 dB [17] relative to the single-mode PSOAM wave. As shown in Fig. 11(b), at the SNR of 30.7 dB, the EVM of two channels for MG-MIMO is 16.2% and 17.8%. Fig. 11(c) shows the

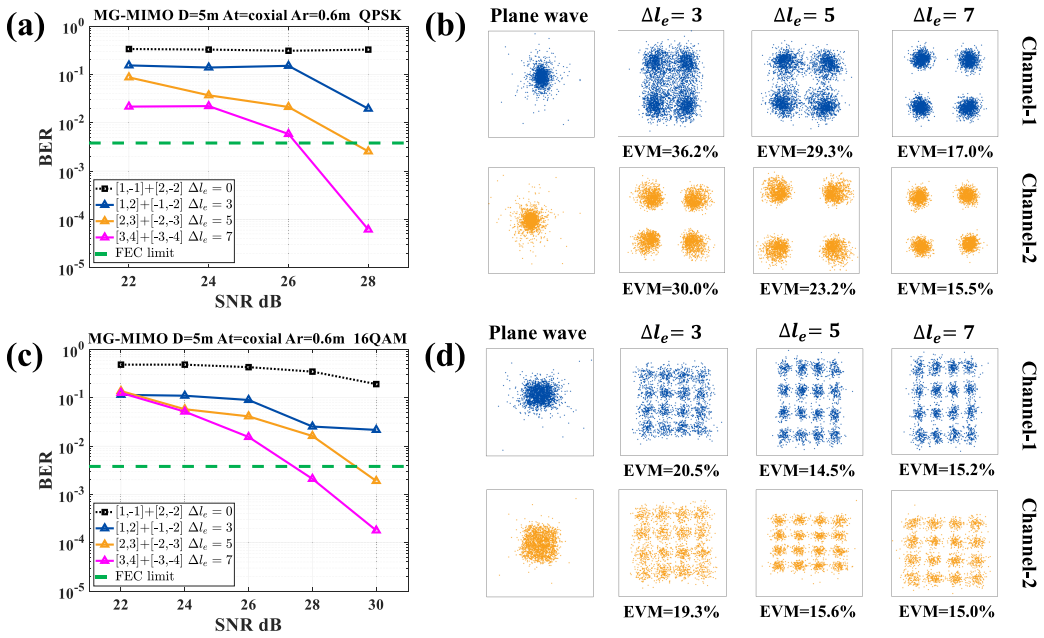

Fig. 9. Experimental results for analyzing the impact on communication link performance of MG's vorticity. The QPSK transmission: (a) measured raw BER performance and (b) typical received constellations with the EVM at a receiving SNR of 28 dB for these four pairs of multiplexed MGs. Likewise, the 16-QAM transmission: (c) measured BER and (d) received constellations with the EVM at a receiving SNR of 30 dB.

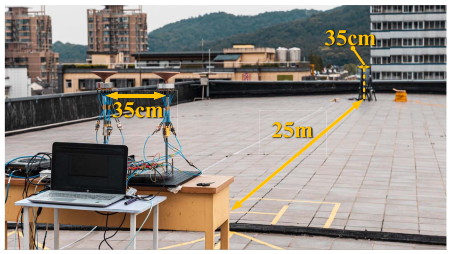

Fig. 10. Experimental setup used to study the impact on communication link performance of MG's directionality.

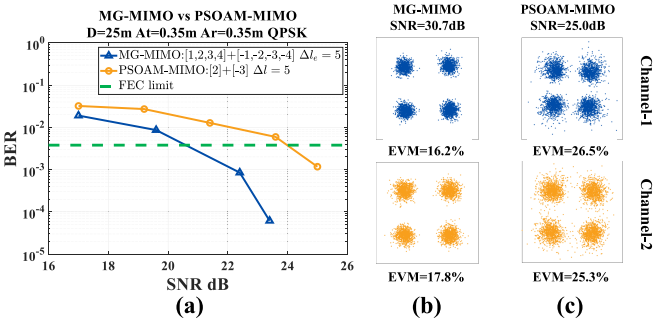

Fig. 11. (a) BER performance of MG-MIMO and PSOAM-MIMO for the QPSK transmission. When the power of transmitting IF signal, the LO power, and the gain of receiving LNA are, respectively, set as −24 dBm, 10 dBm, and 67 dB, the measured receiving SNRs for MG-MIMO and PSOAM-MIMO link are 30.7 and 25 dB, respectively. (b) Received constellations of the former at the corresponding SNR. (c) Received constellations of the latter at the corresponding SNR.

EVM performance of two channels for PSOAM-MIMO, which are 26.5% and 25.3% at the SNR of 25 dB.

Likewise, Fig. 12(a) shows the measured raw BER curves of MG-MIMO and PSOAM-MIMO system for the 16-QAM transmission. MG-MIMO can reach the FEC limit at the receiving SNR of 28 dB. In terms of the existing experimental architecture, PSOAM-MIMO is no longer available for reaching the FEC limit owing to the lower SNR. When the power of transmitting IF signal, the LO power, and the gain of receiving LNA are, respectively, set as −27 dBm, 10 dBm, and 67 dB, the attainable SNR of MG-MIMO link is 28 dB, and this value of PSOAM-MIMO is only 23.6 dB. Here, due to the higher peak-to-average ratio of 16-QAM, in order to avoid the nonlinear distortion [43] caused by the RF amplifier, the power of transmitting IF signal is appropriately reduced to −27 dBm. As shown in Fig. 12(b), at the certain SNR of 28 dB, the EVM of two channels for MG-MIMO is 13.7% and 15.7%. Meanwhile, as we can see from Fig. 11(c), the EVM performance for PSOAM-MIMO is 22.8% and 20.0% at the certain SNR of 23.6 dB.

C. Orthogonality Between Multiplexed MGs Under PASR Scheme

According to (4), if the total number Q and the mode interval Δl of multiplexed MGs are the same, the generated beams will have the same azimuthal intensity pattern. For the case of $\Delta l = 1$, the realized high-gain pencil beams present a spiral phase distribution within the main lobe. Based on the phase information, in virtue of the partial arc sampling receiving (PASR) scheme [44], we can utilize the method of analog phase shift to demultiplex data streams orthogonally with a low complexity. In order to use PASR scheme, the number of multiplexed MGs should be equal to the number of receiving antennas and the receiving antennas need to be placed uniformly at the equal-gain position within MG's main lobe. For $2\pi/\delta$ azimuthal arc and N_r receiving antennas, the angle difference between neighboring antennas meets $2\pi/(\delta N_r)$. If $\Delta l_e^{n_1\ n_2} = l_e^{n_1} - l_e^{n_2}$ is equal to $k'\delta$, where k' is a nonzero integer, the multiplexed $\mathrm{MG}^{\mathrm{n1}}$ and $\mathrm{MG}^{\mathrm{n2}}$ can

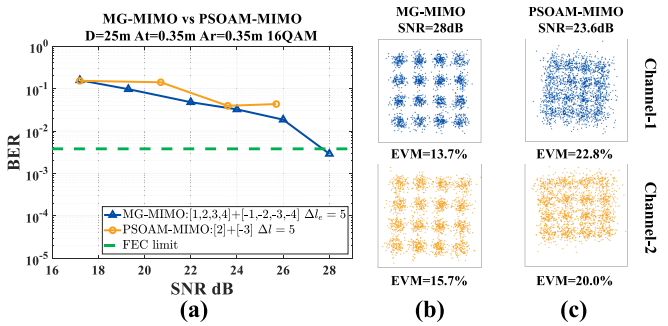

Fig. 12. (a) BER performance of MG-MIMO and PSOAM-MIMO for the 16-QAM transmission. When the power of transmitting IF signal, the LO power, and the gain of receiving LNA are, respectively, set as −27 dBm, 10 dBm, and 67 dB, the measured receiving SNRs for MG-MIMO and PSOAM-MIMO link are 28 and 23.6 dB, respectively. (b) Received constellations of the former at the corresponding SNR. (c) Received constellations of the latter at the corresponding SNR.

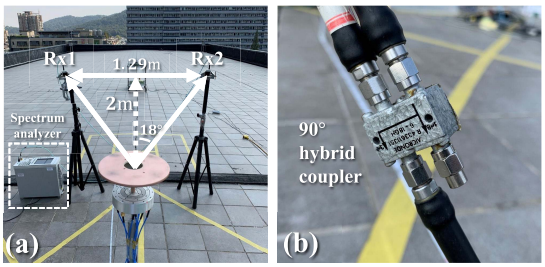

Fig. 13. (a) Experimental setup used to evaluate the orthogonality between multiplexed MGs under PASR scheme. (b) 90° hybrid coupler is used to realize the operation of analog phase shifting at the receiving end.

be demultiplexed orthogonally [26]

$$\sum_{n_r=1}^{N_r} BP_{\mathrm{MG^{n1}}}\left(\frac{2\pi n_r}{\delta N_r}\right) BP^{*}_{\mathrm{MG^{n2}}}\left(\frac{2\pi n_r}{\delta N_r}\right) = \gamma \sum_{n_r=1}^{N_r} e^{-j\cdot\frac{2\pi n_r}{N_r}\cdot\frac{l_e^{n1}-l_e^{n2}}{\delta}} = 0 \quad (7)$$

where γ contains all constant factor. From (7), the angle difference between the adjacent receiving antennas is limited by the Δl_e between multiplexed MGs, and in other words, PASR scheme needs a specific receiving aperture A_r. For the case of two MGs multiplexing, which are MG$\{-4, -3, -2, -1\}$ and MG$\{1, 2, 3, 4\}$ with Δl_e of 5, the specific A_r [26] can be described as

$$A_r = 2D \cdot \tan\left(\frac{\varphi_s}{2}\right) = 2D \cdot \tan\left(\frac{\pi}{2\Delta l_e}\right) \quad (8)$$

where φ_s is the angle difference in azimuthal direction between the neighboring receiving antennas. Fig. 13(a) shows the corresponding experimental setup; when D is set as 2 m, the angle difference between the neighboring antennas can be calculated according to (8), and its value is equal to 36°, so A_r should be set as 1.29 m.

In this experiment, the orthogonality can be characterized by measuring the crosstalk (CT) [7], [8] between two MGs. At the transmitting end, a 10.202 GHz CW signal with the power of 10 dBm is fed to MG$\{1, 2, 3, 4\}$, and the other 10.203 GHz CW signal with the same power is fed to MG$\{-4, -3, -2, -1\}$. At the receiving end, utilizing the

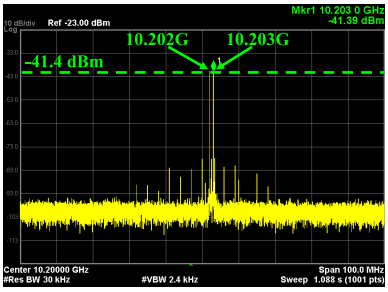

Fig. 14. Without the operation of analog phase shift, the received signals at Rx1 and the result is consistent at Rx2. The key setting parameters of spectrum analyzer: the center frequency (CF) is set as 10.2 GHz, the span is set as 100 MHz, the resolution bandwidth (RBW) is set as 30 kHz, and the video bandwidth (VBW) is set as 2.4 kHz.

TABLE II
MEASURED POWER TRANSFER MATRIX UNDER PASR SCHEME

Received power (dBm)	[Rx1-0°,Rx2-90°]	[Rx1-90°,Rx2-0°]
Tx: 10.202 GHz	-39.82	-62.9
Tx: 10.203 GHz	-60.39	-40.8
CT (dB)	**-20.57**	**-22.1**

PASR scheme, a 2×2 power transfer matrix could be obtained by measuring the power of both received signals with the help of spectrum analyzer (Agilent N9020A). Furthermore, the CT between multiplexed MGs can be calculated by adding the received power of all other MGs (unexpected) and dividing it by the received power of the corresponding MG (expected). For instance, to calculate the CT of MG$\{1, 2, 3, 4\}$, the received power $P_{unexpected}$ of MG$\{-4, -3, -2, -1\}$ should be measured and then divided by the received power $P_{expected}$ of MG$\{1, 2, 3, 4\}$, and it can be given by

$$CT = \frac{P_{unexpected}}{P_{expected}}. \quad (9)$$

According to [44], the phase shift is set as 0° at Rx1 and 90° at Rx2 to demultiplex MG$\{1, 2, 3, 4\}$. Meanwhile, the phase shift is set as 90° at Rx1 and 0° at Rx2 to demultiplex the other one. Here, as shown in Fig. 13(b), the 90° hybrid coupler is used to achieve the corresponding analog phase shift. Certainly, the same functionality can be realized by combining the power combiner and adjustable phase shifter. If the analog phase shift based on the PASR scheme is not operated, as shown in Fig. 14, the power level of two CW signals is all maintained around −41.4 dBm. In virtue of PASR scheme, Fig. 15(a) shows the demultiplexing of MG$\{1, 2, 3, 4\}$ carrying 10.202 GHz CW signal, and its measured intensity is −39.82 dBm, while the intensity of 10.203 GHz CW is suppressed to −60.39 dBm. In addition, Fig. 15(b) shows the demultiplexing of MG$\{-4, -3, -2, -1\}$ carrying 10.203 GHz CW signal, and its measured intensity is −40.8 dBm. Conversely, the intensity of 10.202 GHz CW is suppressed to −62.9 dBm. Table II shows the measured power transfer matrix, and the CT of both the CW signals is below −20 dB. Therefore, it has been proved that the isolation under PASR scheme between two MGs is at least 20 dB and multiplexed MGs have orthogonality to some degree.

Unfortunately, for a long-distance transmission and such a low Δl_e, the PASR scheme needs a big and exaggerated A_r.

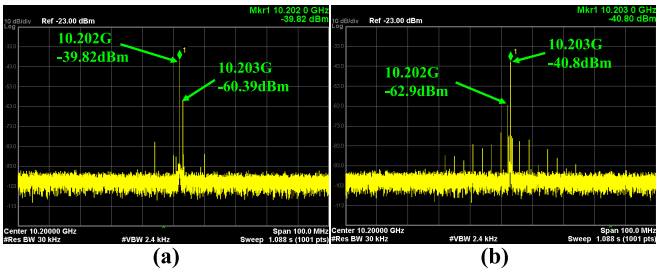

Fig. 15. (a) Using the PASR scheme to demultiplex MG{1, 2, 3, 4} carrying 10.202 GHz CW signal. (b) Using the PASR scheme to demultiplex MG{−4, −3, −2, −1} carrying 10.203 GHz CW signal. The setting parameters of spectrum analyzer remain the same.

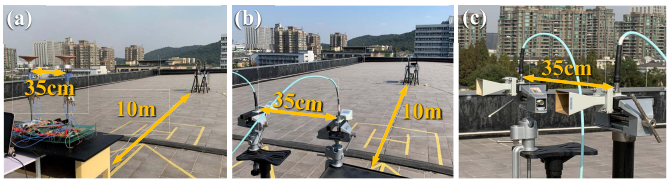

Fig. 16. Comparison between the conventional MIMO and the proposed MG-MIMO. (a) Experimental setup of MG-MIMO link. (b) Experimental setup of MIMO link. (c) Receiving end for both the links.

For example, for the abovementioned two multiplexed MGs, if the communication distance D is extended to 10 m, and the corresponding A_r under PASR scheme will be 6.5 m, which is clearly an unacceptable A_r for practical application. Thus, there is a tradeoff between the receiving complexity and the engineering feasibility. Assuming that two MGs with a Δl_e of 80 can be generated, for the same D of 10 m, the corresponding A_r under PASR scheme could be reduced to 0.4 m. Therefore, it is necessary to generate an MG with higher l_e, and in [25], the partial arc transmitting (PAT) scheme provides a feasible method to achieve this goal.

D. Comparison Between Conventional MIMO and MG-MIMO

In this section, the comparison of communication performance for the conventional MIMO link and the proposed MG-MIMO link has been demonstrated and analyzed under the same channel condition. Fig. 16(a) and (b) shows the experimental setup of the proposed MIMO and the conventional MIMO, respectively. In particular, Fig. 16(c) shows the receiving end setup for both the links. The transmitting end for both links adopts the ULA arraying way, and different from the MG-MIMO, the array element at the transmitting end in MIMO adopts the horn antenna, where the wavefront of the beam generated by the horn can be regarded as an equiphase plane. Therefore, in conventional MIMO, the subchannel difference is only caused by the propagation path difference; in other words, it depends on the aperture of the transceiving end and the communication distance. For the receiving end of both links, two horn antennas are still placed at the symmetry positions along the propagation axis. In MG-MIMO link, a pair of MGs used for this contrast experiment are MG{1, 2, 3, 4} and MG{−4, −3, −2, −1} with Δl_e of 5. The transmitting aperture A_t and receiving aperture A_r of both the systems

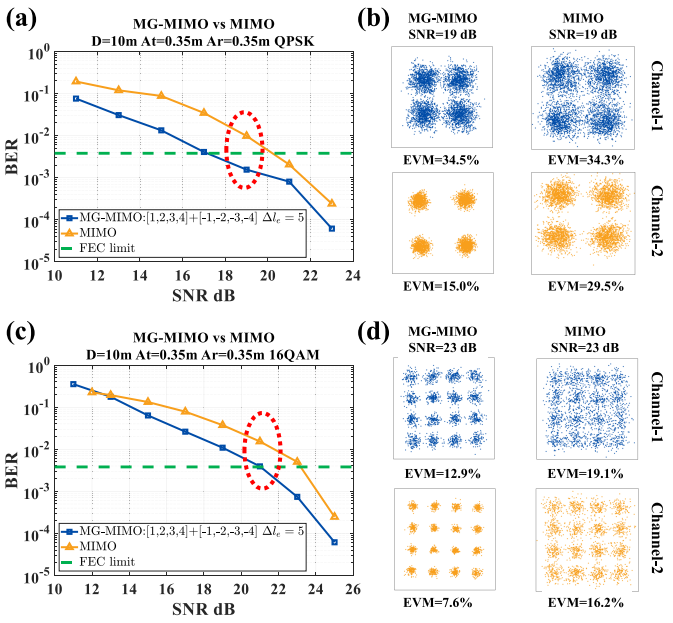

Fig. 17. (a) BER performance of MG-MIMO and MIMO for the QPSK transmission and (b) corresponding received constellations at a receiving SNR of 19 dB. (c) BER performance of MG-MIMO and MIMO for the 16-QAM transmission and (d) corresponding received constellations at a receiving SNR of 23 dB.

are all set as 0.35 m. The communication distance D is set as 10 m. The modulation formats are QPSK, 16-QAM, and 64-QAM. In addition, under such condition, the Rayleigh distance ($2A_r^2/\lambda$) can be calculated as about 8.3 m.

In order to compare the communication performance of MG-MIMO link and MIMO link, the measured raw BER curves of the QPSK transmission and the 16-QAM transmission are shown in Fig. 17(a) and (c), respectively. Besides, Fig. 17(b) shows the typical received constellations with the EVM performance of the QPSK transmission at the same receiving SNR of 19 dB for both the links. Fig. 17(d) shows the corresponding results of the 16-QAM transmission at the same receiving SNR of 23 dB. With the same experimental setup, for both two modulation formats, the MG-MIMO link shows a better BER performance than the MIMO link at the same receiving SNR. Such the improvement comes from the phase control of beam's wavefront manipulated by MG technique, i.e., MG antennas applied for arraying at the transmitting end possess the function of reducing the subchannel correlation, which means that the MG-MIMO system has the potential of long-distance wireless transmission. On the point of reducing the subchannel correlation, the PSOAM-MIMO can also achieve the same effect as the MG-MIMO [22]. However, to our knowledge, the PSOAM-MIMO system has two obvious flaws: one is the deterioration of receiving SNR caused by the waste of energy for the same certain transmitting power and the other is that single-mode PSOAM antenna is lacking in the flexible control [16] of wavefront's phase distribution. In [22], despite showing a better BER performance compared with conventional MIMO, but A_t and A_r of PSOAM-MIMO system are all 0.525 m, the corresponding Rayleigh distance for the operating frequency of 10 GHz is about 18.4 m and its actual transmission distance D is merely 7 m less than half the Rayleigh distance.

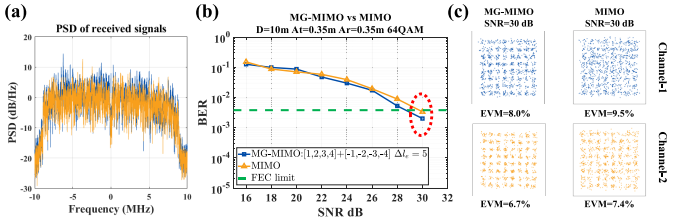

Fig. 18. (a) Typical PSD of the received signals at a receiving SNR of 30 dB for the 64-QAM transmission. (b) Measured BER performance of MG-MIMO and MIMO for the 64-QAM transmission. (c) Corresponding received constellations at a receiving SNR of 30 dB.

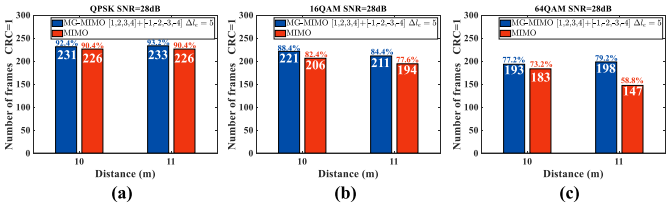

Fig. 19. Results of system robustness testing at a receiving SNR of 28 dB. Both the measuring distances are over the Rayleigh distance. (a) QPSK transmission. (b) 16-QAM transmission. (c) 64-QAM transmission.

For the QPSK transmission, the MG-MIMO link can reach the FEC limit at a lower SNR of about 19 dB, and the conventional MIMO link needs a 21 dB SNR to reach the same limit. Besides, at the same receiving SNR of 19 dB, the EVM of two channels for MG-MIMO is 34.5% and 15.0%, and the EVM performance for MIMO is 34.3% and 29.5%. Furthermore, as far as the test results are concerned, for the 16-QAM transmission, the MG-MIMO link can reach the FEC limit at a lower SNR of about 23 dB, and the conventional MIMO link requires a 25 dB SNR to reach the same limit. At the same receiving SNR of 23 dB, the EVM of two channels for MG-MIMO is 12.9% and 7.6%, and the EVM performance for MIMO is 19.1% and 16.2%.

As for the higher order modulation format, such as the 64-QAM, Fig. 18(a) shows the typical received PSD with a BW of 20 MHz at an SNR of 30 dB. Distinguished from the PSD for lower order modulation formats shown in Fig. 8, the OFDM signal with the 64-QAM modulation format has a higher peak-to-average ratio significantly. The measured raw BER curves of the 64-QAM transmission are shown in Fig. 18(b). Fig. 18(c) shows the received constellations with the measured EVM at the same receiving SNR of 30 dB for both the links. When the actual D exceeds the Rayleigh distance, the correlation between subchannels increases dramatically [19], and the signal multiplexing is becoming more difficult. Compared with the MIMO link, the MG-MIMO link shows a little advantage of BER performance only in the receiving SNR range from 26 to 30 dB. In terms of the experimental results, both the links reach the FEC limit at a receiving SNR of 30 dB. At this SNR, the EVM of two channels for MIMO link is 9.5% and 7.4% because it is merely just over the FEC limit, and the signal clusters of channel-1 are not converged very well. While the MG-MIMO link shows a clearer signal cluster distribution, its corresponding EVM performance is 8.0% and 6.7%. An OFDM symbol consists of 56 subcarriers, of which 52 subcarriers are used for the data transmission in this experiment. Accordingly, like most of practical OFDM systems calculated [8], the attainable spectrum efficiency of the 64-QAM transmission for the MG-MIMO link would be 11.1 bit/s/Hz [6 bits per symbol $\times$ 2 data streams $\times$ (52/56)].

Due to the perturbation and the fading caused by time-varying characteristic of wireless channel [30], even if the test channel is an LoS scenario, the robustness of the proposed MG-MIMO link should be evaluated to analyze the persistence of the systems characteristics. Here, for three modulation formats, we go through the measurement of multiple data frames transmission and then count the number of correctly transmitted frames among them. The cyclic redundancy check [45] algorithm is applied for the receiving end to determine whether a data frame is transmitted correctly. When the value of CRC is equal to 1, it is verified that the data frame transmission is correct. Here, being subject to the RAM limitation of upper computer, the total number of data frames is set as 250.

Fig. 19 shows the robustness testing results for both links at a certain receiving SNR of 28 dB. For each D and each modulation format, when the SNR is fixed, the robustness of MG-MIMO is better than that of MIMO. For the low-order modulation such as QPSK, as D increases, the transmission success rate η_s of both links is maintained at a stable level; when D is 10 m, the η_s of MG-MIMO and MIMO are 92.4% and 90.4%, respectively, and when D is 11 m, this value for both links keep almost unchanged. For the 16-QAM transmission, η_s of both links are all decreased relative to the QPSK transmission; when D is 10 m, the η_s of MG-MIMO and MIMO drop to 88.4% and 82.4%, respectively, and when D is 11 m, this value for both links drops to 84.4% and 77.6%. When it comes to the 64-QAM transmission, although η_s of MG-MIMO has also gone down relative to the 16-QAM transmission, its values maintain the level of 77.2% and 79.2% for a D of 10 and 11 m, respectively, whereas, as D increases, the η_s performance of conventional MIMO deteriorates sharply. When D is 10 m, η_s of MIMO can be more than 70%, and however, when D increases to 11 m, its η_s goes down to 58.8%, which means that nearly half of the data frames are not successfully transmitted.

IV. Demonstration of Long-Distance Transmission Experiment

In this section, we attempt to perform a long-distance MG-MIMO communication link. Both the transmitting and receiving ends are going to adopt the ULA arraying way, A_t and A_r are all set as 0.85 m. For the operating frequency of 10.2 GHz, the corresponding Rayleigh distance ($2A_r^2/\lambda$) can be calculated as about 49 m [35]. In this experiment, the multiplexed PSOAM MGs are MG$\{-4, -3, -2, -1\}$ and MG$\{1, 2, 3, 4\}$ with Δl_e of 5. The modulation formats are QPSK and 16-QAM. The out-door experimental setup of this long-distance transmission is shown in Fig. 20.

Fig. 21(a) shows the measured raw BER curves of this long-distance MG-MIMO link for the QPSK and the 16-QAM transmission. For the QPSK transmission, at a certain receiving SNR of 20 dB, MG-MIMO can reach the FEC limit. Besides, for the 16-QAM transmission, MG-MIMO needs a receiving

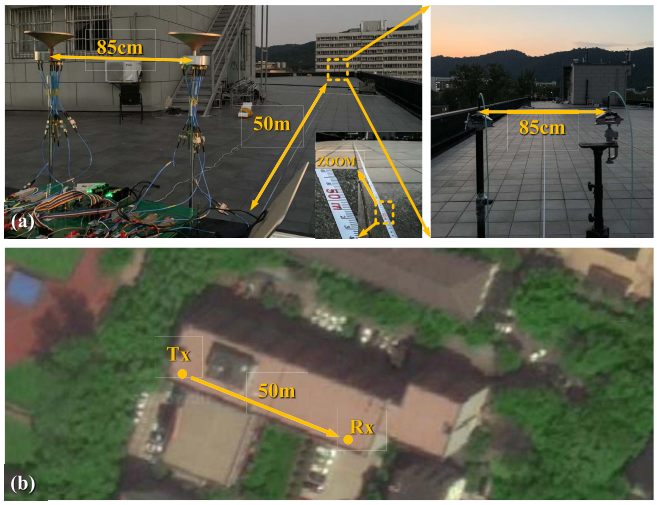

Fig. 20. (a) Experimental setup of the long-distance PSOAM MG-MIMO communication link. The aperture of the transmitting end A_t and the receiving end A_r is all 0.85 m. The operating frequency is 10.2 GHz and the corresponding Rayleigh distance ($2A_r^2/\lambda$) is about 49 m. The actual D is 50 m. (b) Satellite imagery of the experiment site in Hangzhou. The experimental site is selected on a rooftop in order to create a better LoS scene, which is located in Yuquan Campus of Zhejiang University.

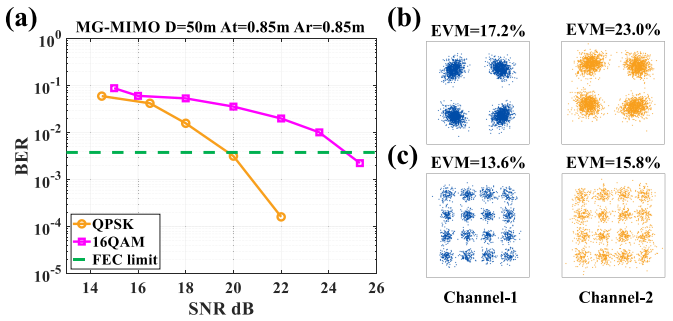

Fig. 21. (a) Measured raw BER curves of MG-MIMO with D of 50 m for the QPSK and the 16-QAM transmission. The typical received constellations with measured EVM performance for (b) QPSK transmission at a receiving SNR of 20 dB and (c) 16-QAM transmission at a receiving SNR of 25.3 dB.

SNR of 25.3 dB to reach the same limit. Moreover, Fig. 21(b) shows the typical received constellations with the measured EVM performance of two channels for the QPSK transmission. At a receiving SNR of 20 dB, the EVM of two channels for the QPSK transmission is 17.2% and 23.0%. Meanwhile, Fig. 21(c) shows the corresponding received constellations for the 16-QAM transmission, and at a receiving SNR of 25.3 dB, the measured EVM of two channels is 13.6% and 15.8%. With the same communication architecture of the preceding proof-of-principle experiments, the attainable spectrum efficiency of the QPSK and the 16-QAM transmission is 3.7 bit/s/Hz [2 bits per symbol $\times$ 2 data streams $\times$ (52/56)] and 7.4 bit/s/Hz [4 bits per symbol $\times$ 2 data streams $\times$ (52/56)].

In addition, it is necessary to set a baseline for comparison. According to the excellent work in [9], NTT Corporation has successfully performed an OAM multiplexing transmission link at a distance of 100 m. Its operating frequency is 40 GHz, and its A_t and A_r are all set as 1.2 m, so the corresponding Rayleigh distance D_R is equal to 384 m. The actual D is about $0.26D_R$. Due to their strong engineering capability in industry, they have implemented 15 streams multiplexing, and the single-way spectrum efficiency is calculated as 4.4 bits/s/Hz/stream. As for our experimental link, the highest order modulation format that can be transmitted is the 16-QAM, and the attainable single-way spectrum efficiency is 3.7 bits/s/Hz/stream. However, for D of 50 m, the physical aperture A_r of 0.85 m, and the operating frequency of 10.2 GHz, our achievable communication distance is about $1.02D_R$ (D_R = 49 m), which means that the MG technique may possess potential in applying to the long-distance point-to-point wireless backhaul communication.

V. Conclusion

In this article, we have demonstrated a series of proof-of-principle experiments of MG-MIMO system to verify and evaluate the reduction of spatial correlation caused by the MG's vorticity, the SNR improvement caused by the MG's beam directionality gain, the orthogonality between multiplexed MGs under PASR scheme, and the better robustness than conventional MIMO when it comes to a communication distance beyond Rayleigh distance. Besides, a tentative long-distance transmission link of MG-MIMO system has been carried out at a communication distance of 50 m with the single-way spectrum efficiency of 3.7 bits/s/Hz/stream. Although the research on the MG-based communication technique is still a young-born field, based on the above experimental results, the MG may provide a novel physical layer method to further improve the communication performance in an MIMO system. Especially, it has potential in the long-range wireless backhaul communication link.

The future investigation on the proposed MG-MIMO system can be focused on the following aspects. As for enhancing the spectrum efficiency, we can increase the number of data streams and adopt the higher order modulation formats to achieve the goal, which requires the updating of baseband communication platform and generating more MGs by optimizing antenna design. The abovementioned PASR scheme can demultiplex the MGs with a low signal processing complexity, but from a practical point of view, we need to design and fabricate a new antenna [25] to directly generate an MG with high l_e in place of the superposing method that this article adopts. This work is currently ongoing.

References

[1] M. H. Alsharif, A. H. Kelechi, M. A. Albreem, S. A. Chaudhry, M. S. Zia, and S. Kim, "Sixth generation (6G) wireless networks: Vision, research activities, challenges and potential solutions," *Symmetry*, vol. 12, no. 4, p. 676, Apr. 2020.

[2] C.-X. Wang, J. Huang, H. Wang, X. Gao, X. You, and Y. Hao, "6G wireless channel measurements and models: Trends and challenges," *IEEE Veh. Technol. Mag.*, vol. 15, no. 4, pp. 22–32, Dec. 2020.

[3] S. M. Mohammadi *et al.*, "Orbital angular momentum in radio: A system study," *IEEE Trans. Antennas Propag.*, vol. 58, no. 2, pp. 565–572, Feb. 2010.

[4] L. Allen, M. W. Beijersbergen, R. J. C. Spreeuw, and J. P. Woerdman, "Orbital angular momentum of light and the transformation of Laguerre–Gaussian laser modes," *Phys. Rev. A, Gen. Phys.*, vol. 45, no. 11, p. 8185, Jun. 1992.

[5] F. Tamburini, E. Mari, A. Sponselli, B. Thidé, A. Bianchini, and F. Romanato, "Encoding many channels on the same frequency through radio vorticity: First experimental test," *New J. Phys.*, vol. 14, no. 3, 2012, Art. no. 033001.

[6] Y. Yan *et al.*, "High-capacity millimetre-wave communications with orbital angular momentum multiplexing," *Nature Commun.*, vol. 5, pp. 1–9, Sep. 2014.

[7] X. Hui *et al.*, "Multiplexed millimeter wave communication with dual orbital angular momentum (OAM) mode antennas," *Sci. Rep.*, vol. 5, no. 1, pp. 1–9, Sep. 2015.
[8] W. Zhang *et al.*, "Mode division multiplexing communication using microwave orbital angular momentum: An experimental study," *IEEE Trans. Wireless Commun.*, vol. 16, no. 2, pp. 1308–1318, Feb. 2017.
[9] H. Sasaki, Y. Yagi, T. Yamada, T. Semoto, and D. Lee, "An experimental demonstration of over 100 Gbit/s OAM multiplexing transmission at a distance of 100 m on 40 GHz band," in *Proc. IEEE Int. Conf. Commun. Workshops (ICC Workshops)*, Jun. 2020, pp. 1–6.
[10] R. Chen, W.-X. Long, X. Wang, and L. Jiandong, "Multi-mode OAM radio waves: Generation, angle of arrival estimation and reception with ucas," *IEEE Trans. Wireless Commun.*, vol. 19, no. 10, pp. 6932–6947, Oct. 2020.
[11] R. Chen, H. Zhou, W.-X. Long, and M. Moretti, "Spectral and energy efficiency of line-of-sight OAM-MIMO communication systems," *China Commun.*, vol. 17, no. 9, pp. 119–127, Sep. 2020.
[12] Y. Lei, Y. Yang, Y. Wang, K. Guo, Y. Gong, and Z. Guo, "Throughput performance of wireless multiple-input multiple-output systems using OAM antennas," *IEEE Wireless Commun. Lett.*, vol. 10, no. 2, pp. 261–265, Sep. 2020.
[13] Y. Yang, Y. Gong, K. Guo, F. Shen, J. Sun, and Z. Guo, "Broad-band multiple OAMs' generation with eight-arm archimedean spiral antenna (ASA)," *IEEE Access*, vol. 8, pp. 53232–53239, 2020.
[14] Y. Chen, S. Zheng, X. Jin, H. Chi, and X. Zhang, "Single-frequency computational imaging using OAM-carrying electromagnetic wave," *J. Appl. Phys.*, vol. 121, no. 18, May 2017, Art. no. 184506.
[15] H. Liu, K. Liu, Y. Cheng, and H. Wang, "Microwave vortex imaging based on dual coupled OAM beams," *IEEE Sensors J.*, vol. 20, no. 2, pp. 806–815, Jan. 2020.
[16] S. Zheng *et al.*, "Realization of beam steering based on plane spiral orbital angular momentum wave," *IEEE Trans. Antennas Propag.*, vol. 66, no. 3, pp. 1352–1358, Mar. 2018.
[17] Z. Zhu *et al.*, "A compact pattern reconfiguration antenna based on multimode plane spiral OA," *IEEE Trans. Antennas Propag.*, vol. 69, no. 2, pp. 1168–1172, Feb. 2021.
[18] J. Zheng, S. Zheng, Z. Shao, and X. Zhang, "Analysis of rotational Doppler effect based on radio waves carrying orbital angular momentum," *J. Appl. Phys.*, vol. 124, no. 16, Oct. 2018, Art. no. 164907.
[19] O. Edfors and A. J. Johansson, "Is orbital angular momentum (OAM) based radio communication an unexploited area?" *IEEE Trans. Antennas Propag.*, vol. 60, no. 2, pp. 1126–1131, Feb. 2012.
[20] M. J. Padgett, F. M Miatto, M. P. J. Lavery, A. Zeilinger, and R. W. Boyd, "Divergence of an orbital-angular-momentum-carrying beam upon propagation," *J. Phys.*, vol. 17, Feb. 2015, Art. no. 023011.
[21] Z. Zhang, S. Zheng, Y. Chen, X. Jin, H. Chi, and X. Zhang, "The capacity gain of orbital angular momentum based multiple-input-multiple-output system," *Sci. Rep.*, vol. 6, no. 1, Jul. 2016, Art. no. 25418.
[22] Z. Zhang, S. Zheng, W. Zhang, X. Jin, H. Chi, and X. Zhang, "Experimental demonstration of the capacity gain of plane spiral OAM-based MIMO system," *IEEE Microw. Wireless Compon. Lett.*, vol. 27, no. 8, pp. 757–759, Aug. 2017.
[23] K. Liu, Y. Cheng, H. Wang, and Q. Yang, "An OAM-generating method using density-weighted circular array," in *Proc. 20th Int. Radar Symp. (IRS)*, Jun. 2019, pp. 1–6.
[24] R. M. Fouda, T. C. Baum, and K. Ghorbani, "Quasi-orbital angular momentum (Q-OAM) generated by quasi-circular array antenna (QCA)," *Sci. Rep.*, vol. 8, no. 1, Dec. 2018, Art. no. 8363.
[25] X. Xiong *et al.*, "Direct generation of OAM mode-group and its application in LoS-MIMO system," *IEEE Commun. Lett.*, vol. 24, no. 11, pp. 2628–2631, Nov. 2020.
[26] X. Xiong, S. Zheng, Z. Zhu, X. Yu, X. Jin, and X. Zhang, "Performance analysis of plane spiral OAM mode-group based MIMO system," *IEEE Commun. Lett.*, vol. 24, no. 7, pp. 1414–1418, Jul. 2020.
[27] Y. Shuang, H. Zhao, W. Ji, T. J. Cui, and L. Li, "Programmable high-order OAM-carrying beams for direct-modulation wireless communications," *IEEE J. Emerg. Sel. Topics Circuits Syst.*, vol. 10, no. 1, pp. 29–37, Mar. 2020.
[28] Y. Chen, X. Xiong, Z. Zhu, S. Zheng, and X. Zhang, "Orbital angular momentum mode-group based spatial field digital modulation: Coding scheme and performance analysis," in *Proc. IEEE Int. Conf. Commun. Workshops (ICC Workshops)*, Jun. 2020, pp. 1–4.
[29] J. Zhou, S. Zheng, X. Yu, X. Jin, and X. Zhang, "Low probability of intercept communication based on structured radio beams using machine learning," *IEEE Access*, vol. 7, pp. 169946–169952, 2019.
[30] A. Goldsmith, *Wireless Communications*. Cambridge, U.K.: Cambridge Univ. Press, 2005.
[31] E. A. Lee and D. G. Messerschmitt, *Digital Communication*. Norwell, MA, USA: Springer, 2012.
[32] B. Jack, M. J. Padgett, and S. Franke-Arnold, "Angular diffraction," *New J. Phys.*, vol. 10, no. 10, Oct. 2008, Art. no. 103013.
[33] W. Yu, B. Zhou, Z. Bu, and S. Wang, "Analyze UCA based OAM communication from spatial correlation," *IEEE Access*, vol. 8, pp. 194590–194600, 2020.
[34] W. Yu, W. Rhee, S. Boyd, and J. M. Cioffi, "Iterative water-filling for Gaussian vector multiple-access channels," *IEEE Trans. Inf. Theory*, vol. 50, no. 1, pp. 145–152, Jan. 2004.
[35] C. A. Balanis, *Antenna Theory: Analysis and Design*. Hoboken, NJ, USA: Wiley, 2016.
[36] D. M. Pozar, *Microwave Engineering*. Hoboken, NJ, USA: Wiley, 2011.
[37] Y. Li, S. Zheng, X. Jin, H. Chi, and X. Zhang, "Radiation characteristics of the Lossy traveling-wave circular antenna," in *Proc. Asia–Pacific Microw. Conf. (APMC)*, vol. 1, Dec. 2015, pp. 1–3.
[38] J. Mitola, "Cognitive radio: An integrated agent architecture for software defined radio," Ph.D. dissertation, Roy. Inst. Technol., Stockholm, Sweden, 2000, pp. 271–350.
[39] Q. H. Spencer, A. L. Swindlehurst, and M. Haardt, "Zero-forcing methods for downlink spatial multiplexing in multiuser MIMO channels," *IEEE Trans. Signal Process.*, vol. 52, no. 2, pp. 461–471, Feb. 2004.
[40] *IEEE Standard for Information Technology—Local and Metropolitan Area Networks—Specific Requirements—Part 11: Wireless LAN Medium Access Control (MAC) and Physical Layer (PHY) Specifications Amendment 5: Enhancements for Higher Throughput*, IEEE Standard 802.11n-2009 (Amendment to IEEE Std 802.11-2007 as amended by IEEE Std 802.11k-2008, IEEE Std 802.11r-2008, IEEE Std 802.11y-2008, and IEEE Std 802.11w-2009), 2009, pp. 1–565.
[41] J. Zhao *et al.*, "Programmable time-domain digital-coding metasurface for non-linear harmonic manipulation and new wireless communication systems," *Nat. Sci. Rev.*, vol. 6, no. 2, pp. 231–238, Nov. 2018.
[42] Y. S. Cho, J. Kim, W. Y. Yang, and C. G. Kang, *MIMO-OFDM Wireless Communications With MATLAB*. Hoboken, NJ, USA: Wiley, 2010.
[43] T. G. Pratt, N. Jones, L. Smee, and M. Torrey, "OFDM link performance with companding for PAPR reduction in the presence of non-linear amplification," *IEEE Trans. Broadcast.*, vol. 52, no. 2, pp. 261–267, Jun. 2006.
[44] W. Zhang, S. Zheng, Y. Chen, X. Jin, H. Chi, and X. Zhang, "Orbital angular momentum-based communications with partial arc sampling receiving," *IEEE Commun. Lett.*, vol. 20, no. 7, pp. 1381–1384, Jul. 2016.
[45] G. Castagnoli, S. Bräuer, and M. Herrmann, "Optimization of cyclic redundancy-check codes with 24 and 32 parity bits," *IEEE Trans. Commun.*, vol. 41, no. 6, pp. 883–892, Jun. 1993.

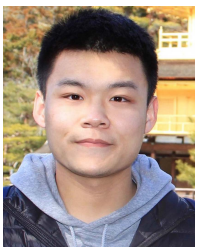

Xiaowen Xiong (Graduate Student Member, IEEE) received the B.S. degree in communication engineering from the Nanjing University of Posts and Telecommunications, Nanjing, China, in 2017. He is currently pursuing the Ph.D. degree in electronic science and technology with Zhejiang University, Hangzhou, China.

His current research interests are in the areas of radio orbital angular momentum (OAM) wave, OAM-based beamforming technique, OAM-based wireless communication system, and signal processing using electromagnetic vortices.

Shilie Zheng (Member, IEEE) received the B.S. and M.S. degrees in materials science and the Ph.D. degree in physical electronics and optoelectronics from Zhejiang University, Hangzhou, China, in 1995, 1998, and 2003, respectively.

In 1998, she joined the Department of Information Science and Electronic Engineering, Zhejiang University, where she was appointed as an Associate Professor in 2005. From November 2005 to March 2006, she spent five months at Tohoku University, Sendai, Japan, as a Research Assistant. From July 2016 to July 2017, she was a Visiting Research Fellow at the RF and Microwave Laboratory, National University of Singapore, Singapore. At the end of 2017, she was appointed as a Full Professor at Zhejiang University. Her current research interests include twisted radio waves and applications, microwave photonics, and wireless communications.

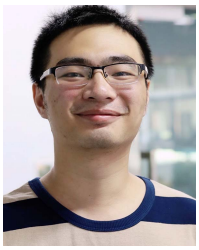

Zelin Zhu (Graduate Student Member, IEEE) received the B.S. degree in electronic information science and technology from the University of Electronic Science and Technology of China, Chengdu, China, in 2018. He is currently pursuing the Ph.D. degree in electronic science and technology with Zhejiang University, Hangzhou, China.

His research interests include vortex electromagnetic wave antenna and its applications in radar systems and communication systems.

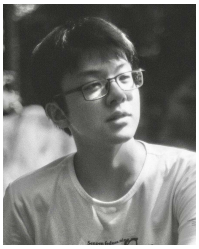

Yuqi Chen (Graduate Student Member, IEEE) received the B.S. degree from the University of Electronic Science and Technology of China, Chengdu, China, in 2019. He is currently pursuing the Ph.D. degree in electronic science and technology with Zhejiang University, Hangzhou, China.

His research interests include orbital angular momentum (OAM) antenna and its applications in wireless communication.

Hongzhe Shi received the B.S. degree in electronic and electrical engineering (EEE) from Central South University, Changsha, Hunan, China, in 2007, and the M.S. degree in data communications and the Ph.D. degree in EEE from the University of Sheffield, Sheffield, U.K., in 2010 and 2014, respectively.

In 2015, he joined Huawei Technologies Company Ltd., Shanghai, China, as a Research Engineer. His research interests include massive-multiple-in–multiple-out (MIMO), AI-MIMO, orbital angular momentum (OAM), and direct antenna modulation.

Bingchen Pan received the B.S. degree in electronic science and technology from Zhejiang University, Hangzhou, China, in 2019, where he is currently pursuing the Ph.D. degree in electronic science and technology.

His research interests include optical true time delay line and its application in the phased array system.

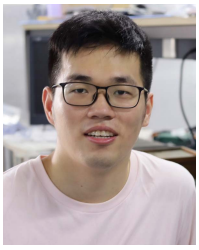

Cheng Ren received the B.S. degree in electronic science and technology from Zhejiang University, Hangzhou, China, in 2019, where he is currently pursuing the master's degree in electronic science and technology.

His research interests include radio-over-fiber technology in optical communication and the application of true time delay line.

Xianbin Yu (Senior Member, IEEE) was a Post-Doctoral Researcher with Tsinghua University, Beijing, China, from 2005 to 2007. Since 2007, he has been with the Technical University of Denmark (DTU), Kongens Lyngby, Denmark, as a Postdoctor, an Assistant Professor, and a Senior Researcher. He is currently a Research Professor at Zhejiang University, Hangzhou, China. He has coauthored two book chapters and more than 180 peer-reviewed international journal articles and conference papers in the area of optical communications. His current research interests are in the areas of THz/microwave photonics and its applications, optical communications, ultrafast photonic RF signal processing, and high-speed photonic wireless access technologies.

Xiaofeng Jin received the B.S. degree in optical engineering from the Huazhong University of Science and Technology, Wuhan, China, in 1990, the M.S. degree in underwater acoustoelectronics engineering from the China Ship Building Institute, Beijing, China, in 1993, and the Ph.D. degree in optical engineering from Zhejiang University, Hangzhou, China, in 1996.

In 1999, he was appointed as an Associate Professor at the Department of Information and Electronic Engineering, Zhejiang University, where he was a Full Professor in 2006. His current research interests include microwave photonics, photonic circuits, components and modules, and smart sensing systems.

Wei E. I. Sha (Senior Member, IEEE) received the B.S. and Ph.D. degrees in electronic engineering from Anhui University, Hefei, China, in 2003 and 2008, respectively.

From July 2008 to July 2017, he was a Post-Doctoral Research Fellow and then a Research Assistant Professor with the Department of Electrical and Electronic Engineering, The University of Hong Kong, Hong Kong. From March 2018 to March 2019, he worked at University College London, London, U.K., as a Marie-Curie Individual Fellow. In October 2017, he joined the College of Information Science and Electronic Engineering, Zhejiang University, Hangzhou, China, where he is currently a tenure-tracked Assistant Professor. His research interests include theoretical and computational research in electromagnetics and optics, focusing on the multiphysics and interdisciplinary research. He has authored or coauthored 150 refereed journal articles, 133 conference publications (including 33 invited talks and two lectures), five book chapters, and two books. His Google Scholar citation is 6270 with H-index of 37. His research involves fundamental and applied aspects in computational and applied electromagnetics, nonlinear and quantum electromagnetics, micro-optics and nano-optics, optoelectronic device simulation, and multiphysics modeling.

Dr. Sha is a member of the Optical Society of America (OSA). He received the Second Prize of Science and Technology from Anhui Province Government, China, in 2015, five best student paper prizes, and the Young Scientist Award with his students. He served as a reviewer for 60 technical journals and a technical program committee member for nine IEEE conferences. He also served as an Associate Editor for IEEE JOURNAL ON MULTISCALE AND MULTIPHYSICS COMPUTATIONAL TECHNIQUES, IEEE OPEN JOURNAL OF ANTENNAS AND PROPAGATION, and IEEE ACCESS.

Xianmin Zhang (Member, IEEE) received the B.S. and Ph.D. degrees in physical electronics and optoelectronics from Zhejiang University, Hangzhou, China, in 1987 and 1992, respectively.

He was appointed as an Associate Professor of information and electronic engineering at Zhejiang University in 1994, where he was a Full Professor in 1999. He was a Research Fellow with The University of Tokyo, Tokyo, Japan, from November 1996 to September 1997, and Hokkaido University, Sapporo, Japan, from October 1997 to September 1998. In 2007, he spent two months with the Research Laboratory of Electronics, Massachusetts Institute of Technology, Cambridge, MA, USA, as a Visiting Research Fellow. He was the Dean of the Department of Information Science and Electronic Engineering, Zhejiang University, from September 2005 to November 2017, the Dean of the School of Micoelectronics, Zhejiang University, from May 2015 to September 2018, the Vice Dean of the Polytechnic Institute, Zhejiang University, from July 2016 to September 2018, the President of the Ningbo Institute of Technology, Zhejiang University, Ningbo, China, from July 2018 to April 2020, and the Dean of Ningbo Campus, Zhejiang University, from September 2018 to November 2020. He is currently the Vice President of NingboTech University, Ningbo. His research interests include microwave photonics, and electromagnetic wave theory and applications.